Comptes Rendus

Mécanique

Dalila Boughazi, Mohammed Debiane and Nabil Allalou

Interfacial capillary–gravity short-crested waves

Research article / *Article de recherche*

Interfacial capillary–gravity short-crested waves

Les ondes à courtes crêtes interfaciales de gravité–capillarité

Dalila Boughazi [a, b]**, Mohammed Debiane**[*, b] **and Nabil Allalou** [b]

[a] Université M'Hamed Bougara, Faculté des Sciences, Siège (Ex. INIL) Boumerdès 35000, Algérie

[b] USTHB, Faculté de physique, BP 32 El Alia Alger, Algérie

E-mails: bouda.2007@hotmail.fr (D. Boughazi), debianemd@yahoo.fr, mddebiane@gmail.com (M. Debiane), n_allalou2004@yahoo.fr (N. Allalou)

Abstract. This paper presents a method derived from Whitham's variational formulation of the problem of interfacial capillary–gravity short-crested waves. It is developed for the resolution of the problem of waves generated by obliquely reflecting interfacial waves from a vertical wall. In essence, Whitham's method is not changed, but computations are performed and arranged to produce a method that has been applied to a number of cases demonstrating the effectiveness and the flexibility of the approach. The performance of the method is illustrated in several examples including the case of harmonic resonance.

Résumé. Cet article présente une méthode dérivée de la formulation variationnelle de Whitham du problème des ondes interfaciales à courte crête de gravité–capillarité. Elle est développée pour la résolution du problème des ondes générées par la réflexion oblique des ondes interfaciales sur une paroi verticale. La méthode de Whitham n'est pas modifiée, mais des calculs sont effectués et organisés pour produire une méthode qui a été appliquée à un certain nombre de cas démontrant l'efficacité et la flexibilité de l'approche. La performance de la méthode est illustrée par plusieurs exemples, y compris le cas de la résonance harmonique.

Keywords. Short-crested interfacial waves, Gravity, Capillarity, Arbitrary depths, Resonance.

Mots-clés. Ondes à courtes crêtes interfaciales, Gravité, Capillarité, Épaisseurs arbitraires, Résonance.

Manuscript received 15 February 2023, revised 17 July 2023, accepted 13 July 2023.

1. Introduction

Over the past decades free surface short crested waves have been studied extensively. These waves are one of the simplest classes of three-dimensional water waves and which are periodic in each of two distinct horizontal directions. They arise at the linear level from the superposition of two progressive wave-trains of equal amplitude and frequency which are propagating

---

* Corresponding author.

at an angle to each other. Starting with the work of Fuchs [1] who obtained second-order so-lutions, approximations through perturbation expansions of higher orders were performed, i.e., by Hsu *et al.* [2], Roberts [3] Ioualalen [4], Kimmoun *et al.* [5], Craig and Nicholls [6, 7]. Roberts and Schwartz [8] and Okamura [9, 10] computed fully numerical short-crested wave solutions. Debiane and Kharif [11] calculated resonant and non-resonant short-crested gravity–capillary waves in deep water using a method derived from Whitham's variational formulation.

While free surface short-crested waves have been extensively studied, relatively little theoret-ical works has been made for internal short-crested waves. To our knowledge, only two stud-ies have been devoted to this field. Allalou *et al.* [12] have investigated numerically fully three-dimensional gravity waves at the interface between two fluids of arbitrary depths confined be-tween two horizontal rigid walls. They computed solutions via a perturbation expansion up to the 27th order in wave steepness. Bocharov *et al.* [13] have numerically solved the weakly non-linear model equation proposed by Khabakhpashev and Tsvelodub [14]. The shapes of station-ary traveling internal waves, both periodic in the two horizontal coordinates and soliton-like, are presented.

Motivated by the efficiency of the method proposed by Debiane and Kharif [11] to the problem of surface short crested waves, we develop here a similar method for the problem of short-crested waves on the interface of a two-layer fluid, in the presence of gravity and surface tension. Even though density stratifications that occur in nature are continuous, it is reasonable to use the two-layer fluid model with a density discontinuity due to its simplicity and the fact that it provides a good approximation when the interfacial wavelength is sufficiently longer than the length scale of the density variation. The study of these waves is the first step to develop an understanding of understanding of little investigated three-dimensional interfacial water waves.

2. The governing equations

We consider short-crested wave field on the interface of a two-layer system of fluids bounded by two rigid horizontal walls. These waves are generated by an interfacial wavetrain of wavelength λ which arrives at some angle of incidence θ on a vertical wall and which is perfectly reflected (Figure 1). θ is the angle between the direction of propagation of the incident wave and the normal to the wall. The resulting waves propagate with constant speed c along the wall. The wavelength in the x-direction is $\lambda_x = \lambda/\sin\theta$ and the wavelength in the y-direction is $\lambda_y = \lambda/\cos\theta$. The fluids are supposed to be homogeneous, incompressible and inviscid, and the motion is assumed to be irrotational. The physical variables associated with the lower fluid are denoted by a subscript (1) and those of the upper fluid by a subscript (2). A cartesian coordinate system $\Re(o, x, y, z)$ is adopted with the x- and y-axis located on the horizontal plane, and the z-axis pointing vertically upwards. The level $z = 0$ coincides with the separation surface between the two layers at rest. All the variables and the equations will be written in dimensionless form in which $K^{-1} = \lambda/2\pi$ and $(gK)^{-1/2}$ are the length and time of reference with K being the wavenumber. It is computationally convenient to use the frame of reference $\Re'(O, X, Y, Z)$, where

$$\begin{pmatrix} X \\ Y \\ Z \end{pmatrix} = \begin{pmatrix} px - \varpi t \\ qy \\ z \end{pmatrix} \tag{1}$$

and in which the short-crested wave is steady with a period of 2π in X and Y. Here ϖ is the non-dimensional frequency and p and q are the non-dimensional wavenumbers in the X and Y directions, respectively, defined by

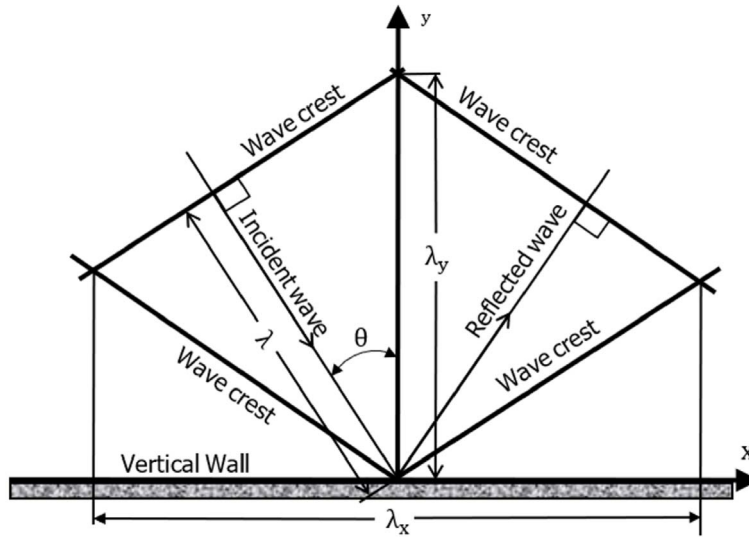$$p = \sin\theta \quad \text{and} \quad q = \cos\theta.$$

Figure 1. Sketch of the reflection of plane wave onto vertical wall at angle θ of incidence.

With the assumptions of incompressibility and irrotational flow in each of the layers, the fluid motions can be described by velocity potentials $\Phi_1(X, Y, Z)$ and $\Phi_2(X, Y, Z)$ in the lower and the upper layers, respectively. These potentials satisfy Laplace's equation in the lower and upper fluid domains

$$p^2\Phi_{iXX} + q^2\Phi_{iYY} + \Phi_{iZZ} = 0 \quad (i = 1, 2). \tag{2}$$

These equations are subject to boundary conditions on the interface between the layers defined by the equation $Z = \eta(X, Y)$

$$-\varpi\eta_X + p^2\eta_X\Phi_{iX} + q^2\eta_Y\Phi_{iY} - \Phi_{iZ} = 0 \tag{3}$$

$$-\frac{\varpi}{\mu-1}(\mu\Phi_{2X} - \Phi_{1X}) + \frac{\mu}{2(\mu-1)}(p^2\Phi_{2X}^2 + q^2\Phi_{2Y}^2 + \Phi_{2Z}^2)$$

$$-\frac{1}{2(\mu-1)}\left(p^2\Phi_{1X}^2 + q^2\Phi_{1Y}^2 + \Phi_{1Z}^2\right) + \eta - \kappa\xi(X, Y) = 0 \tag{4}$$

where

$$\mu = \rho_2/\rho_1 \tag{5}$$

$$\kappa = \frac{TK^2}{g(\rho_1 - \rho_2)} \tag{6}$$

$$\xi(X, Y) = \frac{p^2\eta_{xx}(1 + q^2\eta_Y^2) + q^2\eta_{YY}(1 + p^2\eta_X^2) - 2p^2q^2\eta_{XY}\eta_X\eta_Y}{(1 + p^2\eta_X^2 + q^2\eta_Y^2)^{3/2}}. \tag{7}$$

Here, g is the acceleration of gravity, T the surface tension coefficient, ρ_1 and ρ_2 the densities. Herein, a stable stratification is considered ($\mu < 1$). Equations (3) and (4) are, respectively, the kinematic and the dynamic conditions.

On the solid boundaries, the problem is subjected to impermeability conditions

$$\Phi_z^{(1)} = 0 \quad Z = -d_1, \tag{8}$$

$$\Phi_z^{(2)} = 0 \quad Z = d_2, \tag{9}$$

with lower and upper boundaries at $Z = -d_1$, and $Z = d_2$ respectively ($d_1 > 0, d_2 > 0$).

3. Derivation of the algebraic equations

For irrotational interfacial waves, according to Whitham's method [15], we define the averaged Lagrangian over a rectangular period, as

$$
\overline{L} = \frac{1}{4\pi^2} \int_0^{2\pi} \int_0^{2\pi} \left\{ \frac{1}{1-\mu} \int_{-d_1}^{\eta} \left[-\varpi \frac{\partial \Phi_1}{\partial X} + \frac{1}{2} \left(\vec{\nabla} \Phi_1 \right)^2 \right] dZ \right\} dX dY
$$
$$
+ \frac{1}{4\pi^2} \int_0^{2\pi} \int_0^{2\pi} \left\{ \frac{\mu}{1-\mu} \int_\eta^{d_2} \left[-\varpi \frac{\partial \Phi_2}{\partial X} + \frac{1}{2} \left(\vec{\nabla} \Phi_2 \right)^2 \right] dZ + \frac{1}{2}\eta^2 + \kappa \left(\sqrt{1 + \left(\vec{\nabla}\eta \right)^2} - 1 \right) \right\} dX dY
$$

(10)

with

$$
\vec{\nabla} = \left(p\frac{\partial}{\partial X}, q\frac{\partial}{\partial Y}, \frac{\partial}{\partial Z} \right).
$$

(11)

We seek expressions for $\Phi_1(X,Y,Z)$, $\Phi_2(X,Y,Z)$ and $\eta(X,Y)$ that are doubly periodic functions of the transformed horizontal coordinates. A general representation is

$$
\Phi_1(X,Y,Z) = \sum_{mn} b_{mn} \frac{ch\alpha_{mn}(Z+d_1)}{ch\alpha_{mn}d_1} \chi_{mn}(X,Y)
$$

(12)

$$
\Phi_2(X,Y,Z) = \sum_{mn} c_{mn} \frac{ch\alpha_{mn}(Z-d_2)}{ch\alpha_{mn}d_2} \chi_{mn}(X,Y)
$$

(13)

$$
\eta(X,Y) = \sum_{m=0}^{\infty} \sum_{n=0}^{\infty} \Delta_{m0}\Delta_{n0} a_{mn} \cos mX \cos nY
$$

(14)

where

$$
\chi_{mn}(X,Y) = \sin mX \cos nY
$$

(15)

is introduced for notational convenience to calculate the kinetic energy and

$$
\Delta_{j0} = 1 - \tfrac{1}{2}\delta_{j0}.
$$

Here δ_{j0} is the Kronecker symbol and

$$
\alpha_{mn}^2 = p^2 m^2 + q^2 n^2.
$$

(16)

Substituting expansions (12)–(14) into (10), the averaged Lagrangian $\overline{L}$ is obtained as a function of the unknown coefficients a_{mn}, b_{mn} and c_{mn}. Some details of the calculation of $\overline{L}$ are given in the Appendix A. The resulting averaged Lagrangian is expressed in the following way

$$
\overline{L} = \frac{1}{64(1-\mu)} \sum_{m=1}^{\infty} \sum_{n=0}^{\infty} \sum_{k=1}^{\infty} \sum_{l=0}^{\infty} \frac{b_{mn}b_{kl}}{ch(\alpha_{mn}d_1)ch(\alpha_{kl}d_1)} \times \frac{1}{(\alpha_{mn}+\alpha_{kl})} [_1\Omega_{mnkl}^+]^t [\Theta_{mnkl}^+]
$$
$$
+ \frac{1}{64(1-\mu)} \underbrace{\sum_{m=1}^{\infty} \sum_{n=0}^{\infty} \sum_{k=1}^{\infty} \sum_{l=0}^{\infty}}_{\alpha_{mn}\neq\alpha_{kl}} \frac{b_{mn}b_{kl}}{ch(\alpha_{mn}d_1)ch(\alpha_{kl}d_1)} \times \frac{1}{(\alpha_{mn}-\alpha_{kl})} [_1\Omega_{mnkl}^-]^t [\Theta_{mnkl}^-]
$$
$$
+ \frac{1}{64(1-\mu)} \underbrace{\sum_{m=1}^{\infty} \sum_{n=0}^{\infty} \sum_{k=1}^{\infty} \sum_{l=0}^{\infty}}_{\alpha_{mn}=\alpha_{kl}} \frac{b_{mn}b_{kl}}{ch^2(\alpha_{mn}d_1)} \times [_1\Lambda_{mn}]^t [\Theta_{mnmn}^+]
$$
$$
- \frac{\mu}{64(1-\mu)} \sum_{m=1}^{\infty} \sum_{n=0}^{\infty} \sum_{k=1}^{\infty} \sum_{l=0}^{\infty} \frac{c_{mn}c_{kl}}{ch(\alpha_{mn}d_2)ch(\alpha_{kl}d_2)} \times \frac{1}{(\alpha_{mn}+\alpha_{kl})} [_2\Omega_{mnkl}^+]^t [\Theta_{mnkl}^+]
$$
$$
- \frac{\mu}{64(1-\mu)} \underbrace{\sum_{m=1}^{\infty} \sum_{n=0}^{\infty} \sum_{k=1}^{\infty} \sum_{l=0}^{\infty}}_{\alpha_{mn}\neq\alpha_{kl}} \frac{c_{mn}c_{kl}}{ch(\alpha_{mn}d_2)ch(\alpha_{kl}d_2)} \times \frac{1}{(\alpha_{mn}-\alpha_{kl})} [_2\Omega_{mnkl}^-]^t [\Theta_{mnkl}^-]
$$

$$- \frac{\mu}{64(1-\mu)} \underbrace{\sum_{m=1}^{\infty} \sum_{n=0}^{\infty} \sum_{k=1}^{\infty} \sum_{l=0}^{\infty}}_{\alpha_{mn}=\alpha_{kl}} \frac{c_{mn}c_{kl}}{ch^2(\alpha_{mn}d_2)} \times [_2\Lambda_{mn}]^t [\Theta_{mnmn}^+]$$

$$+ \frac{1}{8} \sum_{m=0}^{\infty} \sum_{n=0}^{\infty} \Delta_{m0}\Delta_{n0}a_{mn}^2 - \frac{1}{4(1-\mu)}\varpi \sum_{m=1}^{\infty} \sum_{n=0}^{\infty} m \frac{b_{mn}}{\alpha_{mn}ch(\alpha_{mn}d_1)} {}_1\omega_{mn}^{mn}$$

$$+ \frac{\mu}{4(1-\mu)}\varpi \sum_{m=1}^{\infty} \sum_{n=0}^{\infty} m \frac{c_{mn}}{\alpha_{mn}ch(\alpha_{mn}d_2)} {}_2\omega_{mn}^{mn} + \frac{\kappa}{4}(R_{00}-4). \tag{17}$$

The quantities $[\Theta_{mnkl}^+]$, $[\Theta_{mnkl}^-]$, $[_i\Omega_{mnkl}^+]$, $[_i\Omega_{mnkl}^-]$, $[_i\Omega_{mn}]$ and $[_i\Lambda_{mn}]$ $(i=1,2)$, are defined in the Appendix A.

According to Whitham's theory, the variational equations to be solved are

$$\frac{\partial \overline{L}}{\partial a_{mn}} = 0 \tag{18}$$

$$\frac{\partial \overline{L}}{\partial b_{mn}} = 0. \tag{19}$$

Applying Equations (18) and (19) to the averaged Lagrangian (17) yields the following set of nonlinear algebraic equations

$$\begin{aligned}
\frac{\partial \overline{L}}{\partial b_{rs}} &= \frac{1}{32(1-\mu)} \sum_{m=1}^{\infty} \sum_{n=0}^{\infty} \frac{b_{mn}}{ch(\alpha_{mn}d_1)ch(\alpha_{rs}d_1)} \times \frac{1}{(\alpha_{mn}+\alpha_{rs})} [_1\Omega_{mnrs}^+]^t [\Theta_{mnsr}^+] \\
&+ \frac{1}{32(1-\mu)} \underbrace{\sum_{m=1}^{\infty} \sum_{n=0}^{\infty}}_{\alpha_{mn}\neq\alpha_{rs}} \frac{b_{mn}}{ch(\alpha_{mn}d_1)ch(\alpha_{rs}d_1)} \times \frac{1}{(\alpha_{mn}-\alpha_{rs})} [_1\Omega_{mnrs}^-]^t [\Theta_{mnrs}^-] \\
&+ \frac{1}{32(1-\mu)} \underbrace{\sum_{m=1}^{\infty} \sum_{n=0}^{\infty}}_{\alpha_{mn}=\alpha_{rs}} \frac{b_{mn}}{ch^2(\alpha_{rs}d_1)} \times [_1\Lambda_{mn}]^t [\Theta_{mnmn}^+] \\
&- \frac{1}{4(1-\mu)}\varpi \sum_{m=1}^{\infty} \sum_{n=0}^{\infty} \frac{r}{\alpha_{rs}ch(\alpha_{rs}d_1)} {}_1\omega_{rs}^{rs} = 0
\end{aligned} \tag{20}$$

$$\begin{aligned}
\frac{\partial \overline{L}}{\partial c_{rs}} &= \frac{1}{32(1-\mu)} \sum_{m=1}^{\infty} \sum_{n=0}^{\infty} \frac{c_{mn}}{ch(\alpha_{mn}d_2)ch(\alpha_{rs}d_2)} \times \frac{1}{(\alpha_{mn}+\alpha_{rs})} [_2\Omega_{mnrs}^+]^t [\Theta_{mnsr}^+] \\
&+ \frac{1}{32(1-\mu)} \underbrace{\sum_{m=1}^{\infty} \sum_{n=0}^{\infty}}_{\alpha_{mn}\neq\alpha_{rs}} \frac{c_{mn}}{ch(\alpha_{mn}d_2)ch(\alpha_{rs}d_2)} \times \frac{1}{(\alpha_{mn}-\alpha_{rs})} [_2\Omega_{mnrs}^-]^t [\Theta_{mnrs}^-] \\
&+ \frac{1}{32(1-\mu)} \underbrace{\sum_{m=1}^{\infty} \sum_{n=0}^{\infty}}_{\alpha_{mn}=\alpha_{rs}} \frac{c_{mn}}{ch^2(\alpha_{rs}d_2)} \times [_2\Lambda_{mn}]^t [\Theta_{mnmn}^+] \\
&- \frac{1}{4(1-\mu)}\varpi \sum_{m=1}^{\infty} \sum_{n=0}^{\infty} \frac{r}{\alpha_{rs}ch(\alpha_{rs}d_2)} {}_2\omega_{rs}^{rs} = 0
\end{aligned} \tag{21}$$

$$\begin{aligned}
\frac{\partial \overline{L}}{\partial a_{rs}} &= \frac{1}{64(1-\mu)} \sum_{m=1}^{\infty} \sum_{n=0}^{\infty} \sum_{k=1}^{\infty} \sum_{l=0}^{\infty} \frac{b_{mn}b_{kl}}{ch(\alpha_{mn}d_1)ch(\alpha_{kl}d_1)} \times \frac{1}{(\alpha_{mn}+\alpha_{kl})} \frac{\partial}{\partial a_{rs}} [_1\overline{\Omega}_{mnkl}^+]^t [\Theta_{mnkl}^+] \\
&+ \frac{1}{64(1-\mu)} \underbrace{\sum_{m=1}^{\infty} \sum_{n=0}^{\infty} \sum_{k=1}^{\infty} \sum_{l=0}^{\infty}}_{\alpha_{mn}\neq\alpha_{kl}} \frac{b_{mn}b_{kl}}{ch(\alpha_{mn}d_1)sh(\alpha_{kl}d_1)} \times \frac{1}{(\alpha_{mn}-\alpha_{kl})} \frac{\partial}{\partial a_{rs}} [_1\Omega_{mnkl}^-]^t [\Theta_{mnkl}^-]
\end{aligned}$$

$$+ \frac{1}{64(1-\mu)} \underbrace{\sum_{m=1}^{\infty}\sum_{n=0}^{\infty}\sum_{k=1}^{\infty}\sum_{l=0}^{\infty}}_{\alpha_{mn}=\alpha_{kl}} \frac{b_{mn}b_{kl}}{ch^2(\alpha_{mn}d_1)} \frac{\partial}{\partial a_{rs}}[_1\Lambda_{mn}]^t[\Theta_{mnmn}^+]$$

$$- \frac{\mu}{64(1-\mu)} \sum_{m=1}^{\infty}\sum_{n=0}^{\infty}\sum_{k=1}^{\infty}\sum_{l=0}^{\infty} \frac{c_{mn}c_{kl}}{ch(\alpha_{mn}d_2)ch(\alpha_{kl}d_2)} \times \frac{1}{(\alpha_{mn}+\alpha_{kl})}\frac{\partial}{\partial a_{rs}}[_2\Omega_{mnkl}^+]^t[\Theta_{mnkl}^+]$$

$$- \frac{\mu}{64(1-\mu)} \underbrace{\sum_{m=1}^{\infty}\sum_{n=0}^{\infty}\sum_{k=1}^{\infty}\sum_{l=0}^{\infty}}_{\alpha_{mn}\neq\alpha_{kl}} \frac{c_{mn}c_{kl}}{ch(\alpha_{mn}d_2)ch(\alpha_{kl}d_2)} \times \frac{1}{(\alpha_{mn}-\alpha_{kl})}\frac{\partial}{\partial a_{rs}}[_2\Omega_{mnkl}^-]^t[\Theta_{mnkl}^-]$$

$$- \frac{\mu}{64(1-\mu)} \underbrace{\sum_{m=1}^{\infty}\sum_{n=0}^{\infty}\sum_{k=1}^{\infty}\sum_{l=0}^{\infty}}_{\alpha_{mn}=\alpha_{kl}} \frac{c_{mn}c_{kl}}{ch^2(\alpha_{mn}d_2)} \times \frac{\partial}{\partial a_{rs}}[_2\Lambda_{mn}]^t[\Theta_{mnmn}^+]$$

$$- \frac{1}{4(1-\mu)}\varpi \sum_{m=1}^{\infty}\sum_{n=0}^{\infty} m\frac{b_{mn}}{\alpha_{mn}ch(\alpha_{mn}d_1)} \frac{\partial}{\partial a_{rs}}(_1\omega_{mn}^{mn})$$

$$+ \frac{\mu}{4(1-\mu)}\varpi \sum_{m=1}^{\infty}\sum_{n=0}^{\infty} m\frac{c_{mn}}{\alpha_{mn}ch(\alpha_{mn}d_2)} \frac{\partial}{\partial a_{rs}}(_2\omega_{mn}^{mn})$$

$$+ \frac{\kappa}{16}\sum_{m=1}^{\infty}\sum_{n=0}^{\infty} a_{mn}|\overline{T}_{mnrs}|^t|\vartheta_{mnrs}| + \frac{1}{4}\Delta_{r0}\Delta_{s0}a_{rs} = 0. \tag{22}$$

4. Numerical procedure

The series in (12)–(14) are truncated at N and the order N is chosen for truncating the other expansions and the series in Equations (20)–(22). The resulting system is to be solved for the unknown a_{mn}, b_{mn}, c_{mn} and ϖ by fixing the values of θ, μ, d_1, d_2 and the steepness which is defined as

$$\varepsilon = \eta(0,0) - \eta(\pi,0) = \sum_{m=0}^{N}\sum_{n=0}^{N} a_{2m+1,2n+1}. \tag{23}$$

Of course, this definition is different from the peak-to-through wave height, since the maximum and minimum points are not always at $(x, y) = (0,0)$ and $(\pi,0)$, respectively.

Note that $a_{00} = 0$, the mean surface level being at $Z = 0$ and, owing to the triangular symmetry of a short-crested wave,

$$a_{mm} = b_{mn} = c_{mm} = 0 \quad \text{when } m + n \text{ is odd.} \tag{24}$$

The system of equations (20)–(23) is solved by Newton's method. In many practical computations it has been found that less than five iterations are sufficient to satisfy the system of equations with an error less than 10^{-14}. Of course, the required number of iterations depends on the configuration studied and on the desired accuracy. For instance, this is the case when we have a slow decay of the Fourier coefficients. To get convergent series it is necessary to increase the number of coefficients, which causes higher computational coasts. Decreasing the order of the truncated series often results in increasing the number of iterations.

The initial estimates for the Newton iteration are given for small amplitudes by analytical solutions calculated up to the "fifth-order" using a perturbation procedure and the computer algebra system MAPLE for symbolic computation.

The Fourier coefficients introduced for the purposes of the present method are computed using the fast Fourier transform (FFT) algorithm. The computational domain is rectangular, periodic in both directions and discretized with constant steps $\Delta X = \Delta Y = 2\pi/M$. M and N may be chosen with a weak constraint, i.e. $M > 2N$, in order to avoid the aliasing phenomenon.

Table 1. Comparison between computed values of the phase velocity with the present method and those given by Allalou *et al.* [12] for $\varepsilon = 0.01, d_1 = 0.8, d_2 = 1, \theta = 50°, \mu = 0.1$ and 0.5

μ	Present method ($N = 23$)	Perturbation method ($N = 27$)
0.1	0.7443973837	0.7443973838
0.5	0.48129554183	0.48129554186

To check the accuracy of the present method, it was necessary to compare our results with those obtained, in the case of gravity interfacial waves, by Allalou *et al.* [12]. A comparison between computed values of the phase velocity is presented in Table 1. Results using the method just described are in excellent agreement to those of Allalou *et al.* computed via a perturbation expansion up to the 27th order in wave steepness.

5. Results and discussion

To illustrate the performance of the method we shall present examples of fully three-dimensional calculations. An interesting variety of wave patterns emerges, with a distinct change in character as a result of different combinations of wave parameters.

5.1. *Resonant cases*

To find the equation which relates the parameters of short crested waves for which harmonic resonance occurs with respect to the (m, n)th harmonic, we solve the system (2)–(4) by using the classical perturbation method. The perturbation parameter we use is the steepness ε. We expand the quantities Φ_1, Φ_2, η and ϖ as power series in the parameter ε.

$$\Phi_1 = \sum_{r=1} \Phi_1^{(r)} \varepsilon^r \quad \Phi_2 = \sum_{r=1} \Phi_2^{(r)} \varepsilon^r \quad \eta = \sum_{r=1} \eta^{(r)} \varepsilon^r \quad \varpi = \sum_{r=0} \varpi_r \varepsilon^r. \tag{25}$$

The dimensionless velocity potentials at the free surface are expressed in terms of the Taylor expansions at $Z = 0$ instead of $Z = \eta(X, Y)$:

$$\Phi_i(X, Y, Z = \eta(X, Y)) = \Phi_i(X, Y, 0) + \left.\frac{\partial \Phi_i}{\partial Z}\right|_{Z=0} \eta + \left.\frac{\partial^2 \Phi_i}{\partial Z^2}\right|_{Z=0} \frac{\eta^2}{2!} + \left.\frac{\partial^3 \Phi_i}{\partial Z^3}\right|_{Z=0} \frac{\eta^3}{3!} + \cdots. \tag{26}$$

As did Kimmoun *et al.* [5], $\xi(X, Y)$ is written in this form

$$\xi(X, Y) = \frac{N(X, Y)}{(1 + D(X, Y))^{3/2}} \tag{27}$$

with

$$N(X, Y) = p^2 \eta_{XX}(1 + q^2 \eta_Y^2) + q^2 \eta_{YY}(1 + p^2 \eta_X^2) - 2p^2 q^2 \eta_{XY} \eta_X \eta_Y$$

and

$$D(X, Y) = p^2 \eta_X^2 + q^2 \eta_Y^2$$

$\xi(X, Y)$ is then developed in terms of a series expansion:

$$\xi(X, Y) = N(X, Y) \left[1 - \tfrac{3}{2} D + \tfrac{15}{8} D^2 - \tfrac{105}{48} D^3 + O(D^5) \right]. \tag{28}$$

After substitution into Equations (2)–(4) and gathering the ε of the same power, we get a new set of equations that was processed using the symbolic software package MAPLE. We proceed by seeking solutions of the form

$$\begin{cases} \Phi_1^{(r)} = \sum\sum b_{mn}^{(r)} \sin(mX)\cos(nY)\dfrac{\cosh(\alpha_{mn}(Z+d_1))}{\cosh(\alpha_{mn}d_1)} \\[2mm] \Phi_2^{(r)} = \sum\sum c_{mn}^{(r)} \sin(mX)\cos(nY)\dfrac{\cosh(\alpha_{mn}(Z-d_2))}{\cosh(\alpha_{mn}d_2)} \\[2mm] \eta^{(r)} = \sum\sum a_{mn}^{(r)} \cos(mX)\cos(nY). \end{cases} \tag{29}$$

To determine the resonance condition, one can rewrite the kinematic and dynamical equations, at order (r), as follows

$$\begin{cases} -m\varpi_0 a_{mn}^{(r)} + \alpha_{mn}F_{mn}b_{mn}^{(r)} = A_{mn}^{(r-1)} \\[2mm] -m\varpi_0 a_{mn}^{(r)} - \alpha_{mn}G_{mn}c_{mn}^{(r)} = B_{mn}^{(r-1)} \\[2mm] (\kappa\alpha_{mn}^2 + 1 - \mu)a_{mn}^{(r)} + m\varpi_0(\mu c_{mn}^{(r)} - b_{mn}^{(r)}) = C_{mn}^{(r-1)} \end{cases} \tag{30}$$

where $A_{mn}^{(r-1)}$, $B_{mn}^{(r-1)}$ and $C_{mn}^{(r-1)}$ are terms depending only on coefficients of order $(r-1)$,

$$F_{mn} = \tanh(\alpha_{mn}d_1), \quad G_{mn} = \tanh(\alpha_{mn}d_2) \quad \text{and} \quad \varpi_0^2 = \frac{(1-\mu)(1+\kappa)\tanh(d_1)\tanh(d_2)}{\mu\tanh(d_2)+\tanh(d_1)}. \tag{31}$$

The above system of equations has solutions of the form

$$\begin{cases} a_{mn}^{(r)} = -\dfrac{\alpha_{mn}G_{mn}F_{mn}C_{mn}^{(r-1)} + m\varpi_0\left(G_{mn}A_{mn}^{(r-1)} + \mu F_{mn}B_{mn}^{(r-1)}\right)}{-\alpha_{mn}(\kappa\alpha_{mn}^2+1-\mu)F_{mn}G_{mn} + m^2\varpi_0^2(G_{mn}+\mu F_{mn})} \\[4mm] b_{mn}^{(r)} = \dfrac{m^2\varpi_0^2\mu\left(A_{mn}^{(r-1)}-B_{mn}^{(r-1)}\right) - \alpha_{mn}m\varpi_0 G_{mn}C_{mn}^{(r-1)} - \alpha_{mn}G_{mn}A_{mn}^{(r-1)}(\kappa\alpha_{mn}^2+1-\mu)}{-\alpha_{mn}(\kappa\alpha_{mn}^2+1-\mu)F_{mn}G_{mn} + m^2\varpi_0^2(G_{mn}+\mu F_{mn})} \\[4mm] c_{mn}^{(r)} = \dfrac{m^2\varpi_0^2\left(A_{mn}^{(r-1)}-B_{mn}^{(r-1)}\right) + \alpha_{mn}m\varpi_0 F_{mn}C_{mn}^{(r-1)} + \alpha_{mn}F_{mn}B_{mn}^{(r-1)}(\kappa\alpha_{mn}^2+1-\mu)}{-\alpha_{mn}(\kappa\alpha_{mn}^2+1-\mu)F_{mn}G_{mn} + m^2\varpi_0^2(G_{mn}+\mu F_{mn})}. \end{cases} \tag{32}$$

These coefficients have zero divisors when the parameters of the wave satisfy the relation

$$-\alpha_{mn}(\kappa\alpha_{mn}^2+1-\mu)\tanh(\alpha_{mn}d_1)\tanh(\alpha_{mn}d_2) + m^2\varpi_0^2\left(\tanh(\alpha_{mn}d_2)+\mu\tanh(\alpha_{mn}d_1)\right) = 0. \tag{33}$$

These zero divisors are now recognized to be indicative of the occurrence of harmonic resonances. Physically, the fundamental $(1,1)$ excites the harmonic (m,n) which travels at the same phase speed. Over a long time scale the resonance allows continual redistribution of energy between the fundamental and the resonant harmonic.

Taking advantage of the ability of the present method to provide the properties of the fully resonant waves, it is natural to examine these resonances. Taking $m = n = 2$, $d_1 = d_2 = 0.5$, $\theta = 48°$ and $\mu = 0.07$, Equation (33) yields $\kappa = 0.07587182693956657\ldots$. As known, such a resonance gives rise to a multiplicity of solutions. In our case, we obtain three solution branches; two of them being connected through a turning point which occurs at about $\varepsilon = 0.009$, as shown in Figure 2. The latter exhibits the multiple solution structure of the wave speed as a function of steepness. The starting point of branch (1) was generated from a non resonant solution computed with $\kappa = 0.08$ varying progressively κ from this value to 0.07587182693956657 by step not exceeding few percents of the fixed value. Figure 3 shows the shape of this family of short-crested waves.
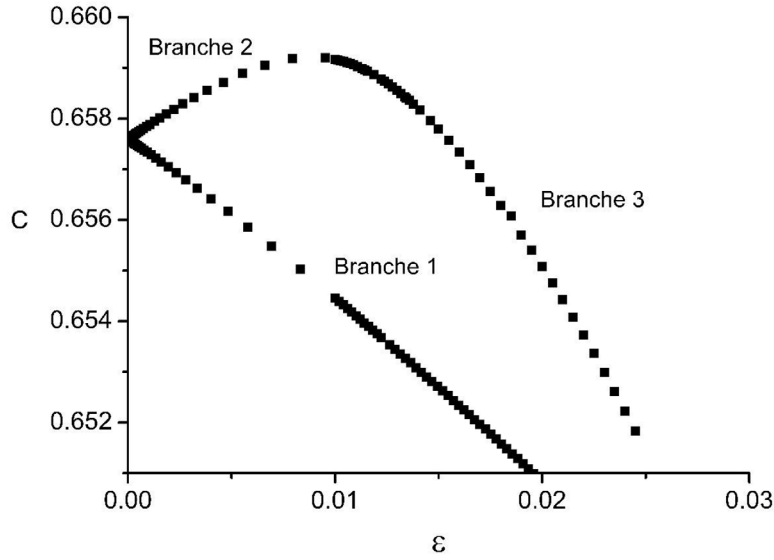
Figure 2. Variation of wave speed with steepness for three-dimensional Wilton ripples.

The lines of the intersection with the planes $X = 2\pi$ or $Y = 0$ (remind that the patterns are 2π-periodic in the both directions) have the same shape as the profile of Wilton type 1 ripples [16]: they exhibit secondary troughs in the crests. The starting point of branch (2) was obtained, for small values of the wave steepness, by taking $\kappa = 0.07587182693956657$. Figure 4 shows that the lines of the intersection of their shape with the planes $X = 2\pi$ or $Y = 0$ are similar to the profile of the so-called Wilton type 2 ripples, that is to say, secondary crests of a substantial height appear in the troughs. Beyond the turning point, we have a mixed-type solution which combines the latter two patterns. Figure 5 shows the shape of these waves which exhibits secondary troughs in the crests and similarly secondary crests in the troughs.

5.2. *Energies*

Once the coefficients a_{mn}, b_{mn} and c_{mn} determined, it is straightforward to compute kinetic and potential energies by using the expressions (A9), (A10) and (A13) given in the Appendix A. As an illustration we present the results obtained for the resonant cases discussed above. The mean kinetic- and potential-energy densities for the wave referred to as type 1 are plotted in Figure 6. Those of the cases referred to as type 2 and type 3 are plotted in Figure 7. In Figure 8, the energy densities of the wave of type 2 correspond to $\varepsilon < 0.009$ and those of the wave of type 3 to $\varepsilon > 0.009$. For all the cases presented in these two figures, the kinetic-energy density is larger than the two potential-energy densities. There are configurations for which potential-energy density, V_g, is greater than the kinetic-energy, as shown in Figure 8. However, we did not find any cases where the capillary-potential-energy density, V_τ, is greater than the other two energy densities.

5.3. *Square waves*

When one layer is shallow and the other is deep, the wave profile is generally more sharply peaked on the side pointing into the deeper layer. When the lower fluid has a very small depth and the upper fluid is deep, it will be possible to obtain strongly localized shapes similar to grid waves
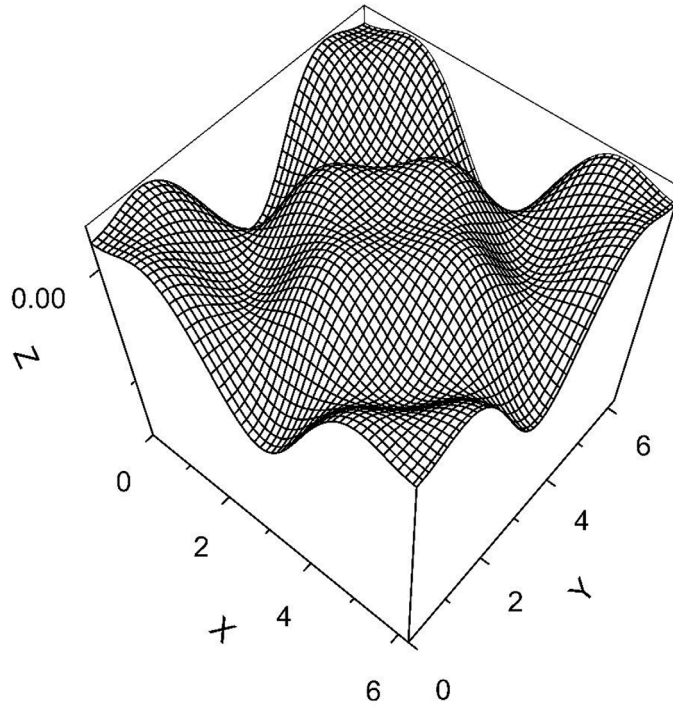
Figure 3. Three-dimensional Wilton ripples of the type 1 for $d_1 = d_2 = 0.5$, $\theta = 48°$, $\mu = 0.07$ and $\kappa = 0.07587182693956657$.
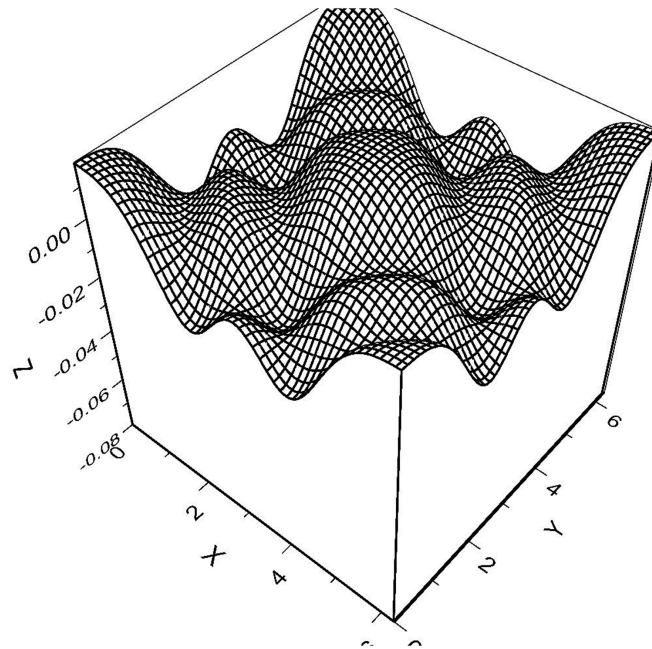

Figure 4. Three-dimensional Wilton ripples of type 2 for $d_1 = d_2 = 0.5$, $\theta = 48°$, $\mu = 0.07$ and $\kappa = 0.07587182693956657$.
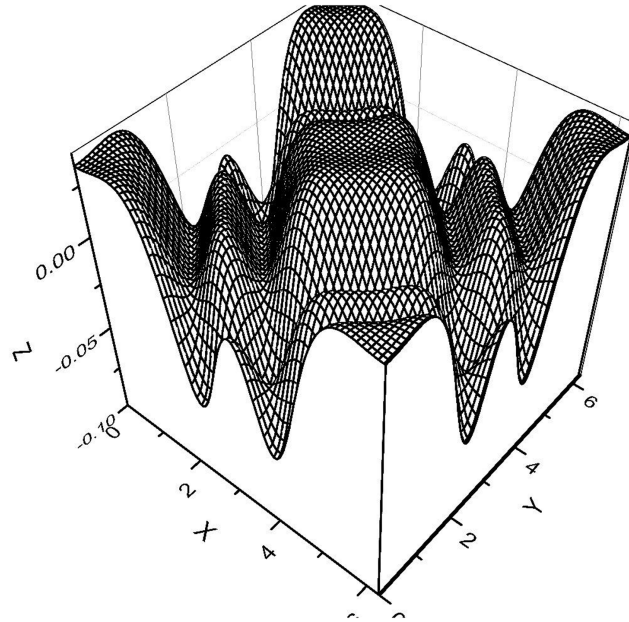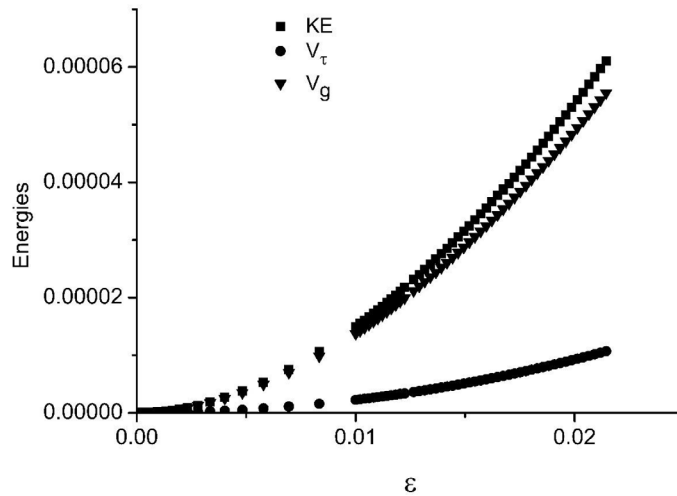
Figure 5. Three-dimensional Wilton ripples of type 3 for $d_1 = d_2 = 0.5$, $\theta = 48°$, $\mu = 0.07$ and $\kappa = 0.07587182693956657$.

Figure 6. Variation of mean kinetic energy density (KE), mean gravity-potential-energy density (V_g) and mean capillary-potential-energy density with steepness for three-dimensional Wilton ripples of type 1.

that form square-shaped patterns like those shown in Figure 9. A similar surface wave pattern has been photographed by Terry Toedte-Meier off the coast of Oregon (cf. Segur [17]). Solutions in the form of grid waves can be treated as a composition of two plane solitary waves propagating at right angles to each other. Each wave train exhibits flat-trough, sharp-crest pattern, but successive wave crests in the same train are so far apart that each crest behaves nearly like a solitary wave. At the intersections of the crests appear peaks of greater elevation. The flatness
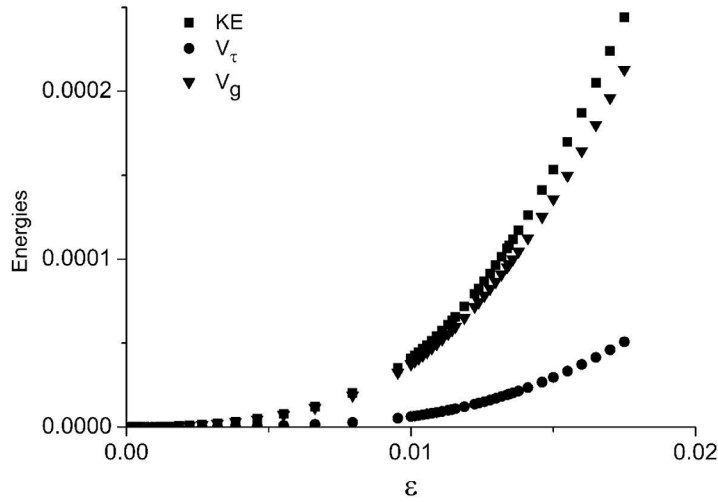
Figure 7. Variation of mean kinetic energy density (KE), mean gravity-potential-energy density (V_g) and mean capillary-potential-energy density with steepness for three-dimensional Wilton ripples of the type 2 and of the type 3.
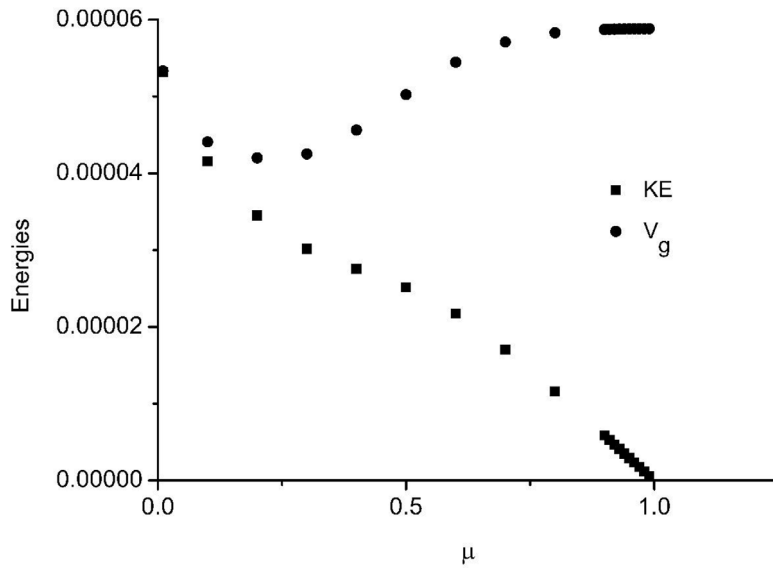

Figure 8. Variation of mean kinetic energy density (KE) and mean gravity-potential-energy density (V_g) with the density ratio μ for $d_1 = d_2 = 0.1$, $\theta = 50°$, $\varepsilon = 0.02$ and $\kappa = 0$.

of the trough is due to effects from the bottom and may indicate that these solutions are more nonlinear. If, on the contrary, it is the upper layer that is shallow and the lower layer is deep, we obtain similar square-shaped patterns, but their convex sides are oriented upward as shown in Figure 10. These two families of waves are obtained more easily with very low values of μ and κ. Their chapes changes as we increase these two parameters.

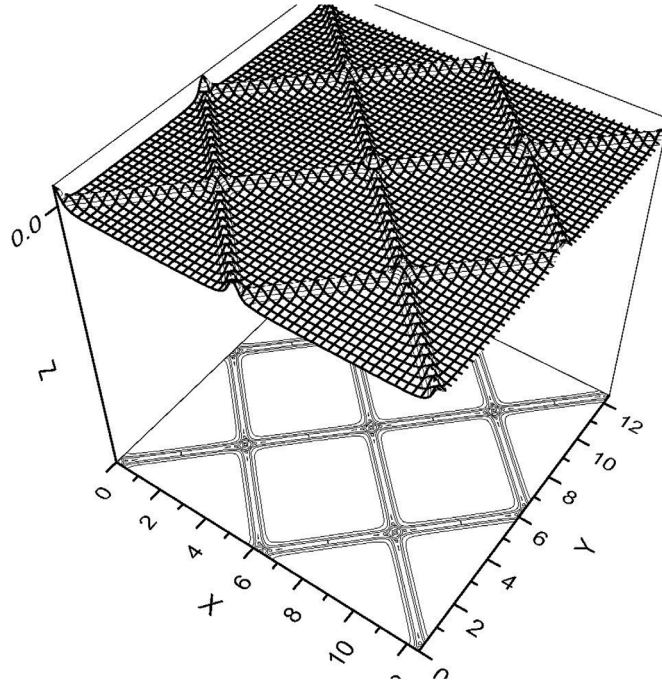**Figure 9.** Graph in perspective of square waves with their convex sides oriented downward for $d_1 = 0.034, d_2 = 0.1, \theta = 1°, \varepsilon = 0.02, \mu = 0.1$ and $\kappa = 0$. The vertical scale is enlarged to emphasize the shape.
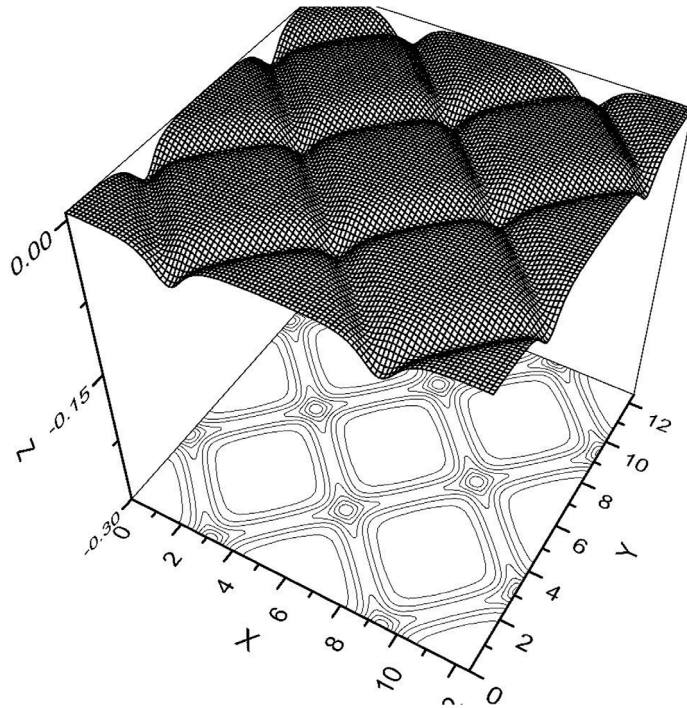

Figure 10. Graph in perspective of square waves with their convex sides oriented upward for $d_1 = 5$, $d_2 = 0.02$, $\theta = 1°$, $\varepsilon = 0.02$, $\mu = 0.1$ and $\kappa = 0$. The vertical scale is enlarged to emphasize the shape.
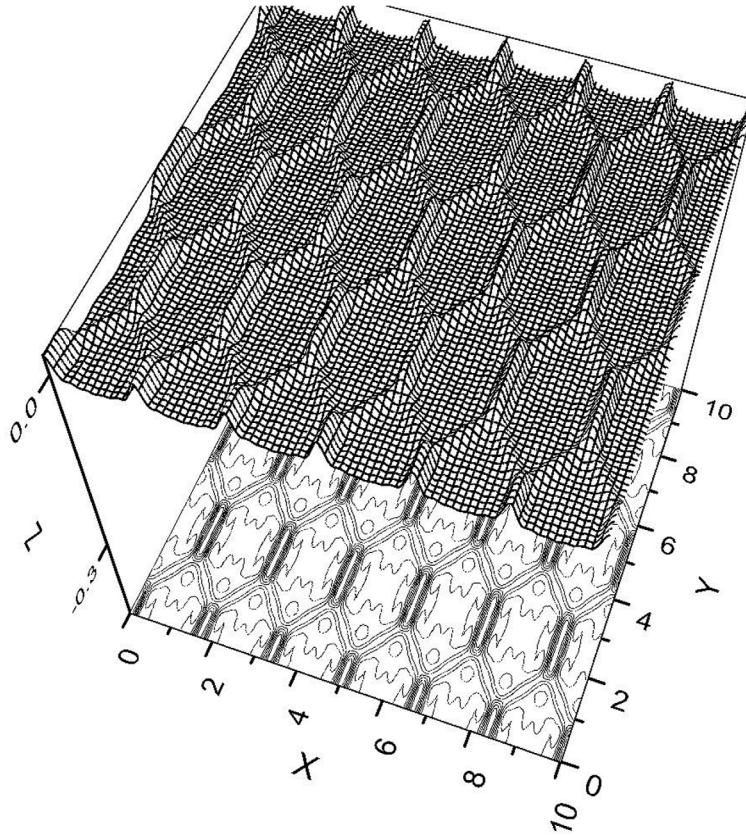
Figure 11. Graph in perspective of hexagonal waves with their convex sides oriented downward for $d_1 = 0.034$, $d_2 = 0.1$, $\theta = 5°$, $\varepsilon = 0.02$, $\mu = 0.1$ and $\kappa = 0$. The vertical scale is enlarged to emphasize the shape.

5.4. *Hexagonal waves*

For low values of θ, our method can generate hexagonal traveling wave solutions. There exist several types of these waves. When the lower fluid has a very small depth and the upper fluid is deep, we can generate honeycomb shapes like those shown in Figure 11. Each cell have a large flat trough which is surrounded by a narrow six sided ridge. The pattern is elongated in the direction perpendicular to the phase velocity. The sides of the ridge which are aligned with the Y-direction are relatively flat over a large fraction of their length and are higher than the other four sides which complete the hexagonal pattern. If it is the upper layer that is shallow and the lower layer is deep, we obtain similar hexagonal patterns but each of them have a large flat crest which is surrounded by a six sided depression boundary (see Figure 12). Figure 13 presents a third notable case example which exhibit mixed structures, that is to say they have well-pronounced diamond crests while the troughs have hexagonal patterns. Hexagonal patterns have been observed experimentally by Hammack *et al.* [18].

6. Conclusion

A method has been developed for the solution of the problem involving interfacial capillary–gravity short-crested waves propagating at the interface between two inviscid immiscible fluids
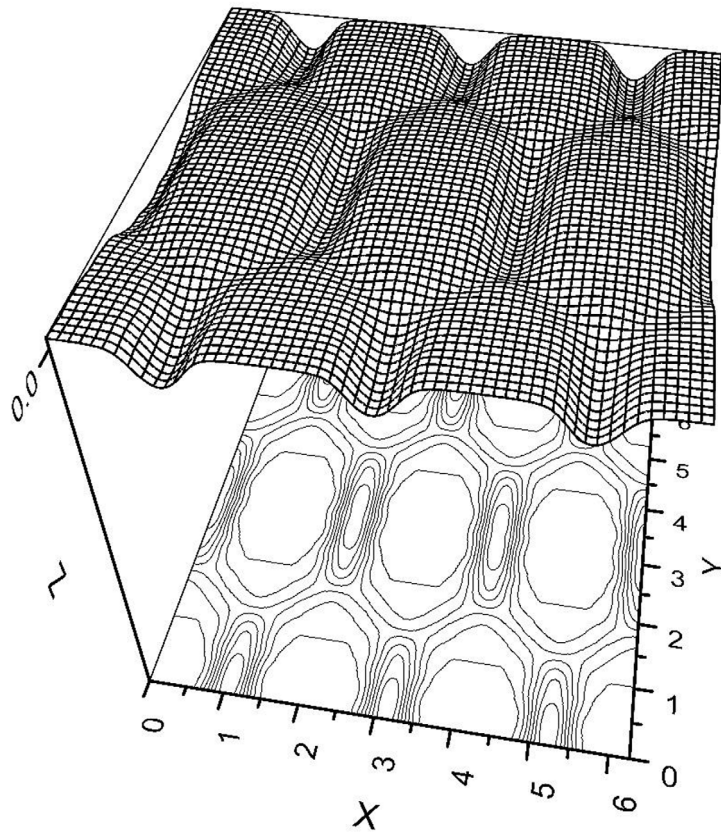
Figure 12. Graph in perspective of hexagonal waves with their convex sides oriented upward for $d_1 = 3$, $d_2 = 0.02$, $\theta = 50°$, $\varepsilon = 0.02$, $\mu = 0.1$ and $\kappa = 0$. The vertical scale is enlarged to emphasize the shape.

of different densities lying between two rigid boundaries. A large number of interesting configurations can be computed using our approach. Several results have been presented to illustrate the effectiveness of our approach. The shapes of these waves depend on different parameters of the problem: the surface tension coefficient, the fluid layer depth, density ratios and the angle between the direction of propagation of the incident wave and the normal to the wall. The influence of these parameters will be further investigated in the future.

Conflicts of interest

Authors have no conflict of interest to declare.
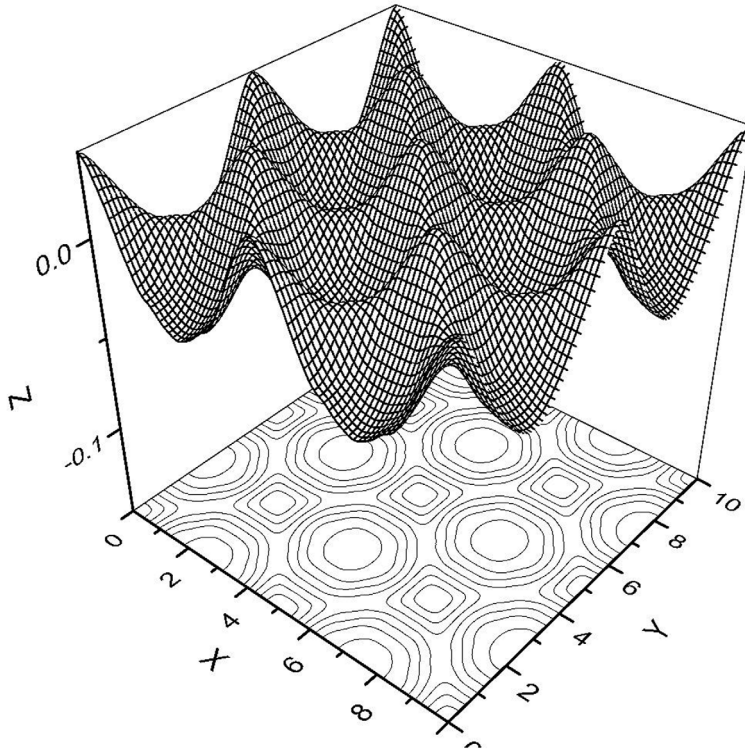
Acknowledgements

Figure 13. Graph in perspective of mixed waves.

Appendix A. Calculation of the averaged Lagrangian $\overline{L}$

This appendix describes some details of the calculation of the averaged Lagrangian $\overline{L}$.

A.1. *The term of kinetic energy*

In the averaged Lagrangian function (10) given in the body of the paper, the contribution of the kinetic energy is

$$\text{KE} = \underbrace{\frac{1}{1-\mu}\frac{1}{8\pi^2}\int_0^{2\pi}\int_0^{2\pi}\int_{-d_1}^{\eta}\left(\vec{\nabla}\Phi_1\right)^2 \text{d}X\text{d}Y\text{d}Z}_{\text{KE}_1} + \underbrace{\frac{\mu}{1-\mu}\frac{1}{8\pi^2}\int_0^{2\pi}\int_0^{2\pi}\int_{\eta}^{d_2}\left(\vec{\nabla}\Phi_2\right)^2 \text{d}X\text{d}Y\text{d}Z}_{\text{KE}_2}. \quad \text{(A1)}$$

The first term on the right-hand side of Equation (A1), labelled KE_1, represents the kinetic energy in the lower fluid of the wave. Substituting expansion (12) into KE_1 leads to

$$\begin{aligned}
\text{KE}_1 = \frac{1}{1-\mu}\frac{1}{8\pi^2}\sum_{m=1}^{\infty}\sum_{n=0}^{\infty}\sum_{k=1}^{\infty}\sum_{l=0}^{\infty}&\left(\frac{b_{mn}b_{kl}}{ch(\alpha_{mn}d_1)ch(\alpha_{kl}d_1)}\right) \\
&\times \int_0^{2\pi}\int_0^{2\pi}\left\{\int_{-d_1}^{\eta}ch(\alpha_{mn}(Z+d_1))ch(\alpha_{kl}(Z+d_1))\text{d}Z\,\vec{\nabla}(\chi_{mn})\cdot\vec{\nabla}(\chi_{kl})\right. \\
&\left.+\alpha_{mn}\alpha_{kl}\int_{-d_1}^{\eta}sh(\alpha_{mn}(Z+d_1))sh(\alpha_{kl}(Z+d_1))\text{d}Z\,\chi_{mn}\chi_{kl}\right\}\text{d}X\text{d}Y. \quad \text{(A2)}
\end{aligned}$$

Using the properties of the products of hyperbolic functions and proceeding in a similar way as in Debiane and Kharif [11], we obtain

$$
\begin{aligned}
\mathrm{KE}_1 &= \frac{1}{1-\mu}\frac{1}{64}\sum_{m=1}^{\infty}\sum_{n=0}^{\infty}\sum_{k=1}^{\infty}\sum_{l=0}^{\infty}\frac{b_{mn}b_{kl}}{ch(\alpha_{mn}d_1)ch(\alpha_{kl}d_1)} \\
&\times \frac{1}{(\alpha_{mn}+\alpha_{kl})}\left\{\begin{array}{l}\left[{}_1P_{k-m,l-n}^{mnkl}(p^2mk+q^2nl+\alpha_{mn}\alpha_{kl})+{}_1P_{k+m,l-n}^{mnkl}(p^2mk-q^2nl-\alpha_{mn}\alpha_{kl})\right.\\ \left.+{}_1P_{k-m,l+n}^{mnkl}(p^2mk-q^2nl+\alpha_{mn}\alpha_{kl})+{}_1P_{k+m,l+n}^{mnkl}(p^2mk+q^2nl-\alpha_{mn}\alpha_{kl})\right]\end{array}\right\} \\
&+ \frac{1}{1-\mu}\frac{1}{64}\sum_{m=1}^{\infty}\sum_{n=0}^{\infty}\sum_{k=1}^{\infty}\sum_{l=0}^{\infty}\frac{b_{mn}b_{kl}}{ch(\alpha_{mn}d_1)ch(\alpha_{kl}d_1)} \\
&\times \frac{1}{(\alpha_{mn}-\alpha_{kl})}\left\{\begin{array}{l}\left[{}_1M_{k-m,l-n}^{mnkl}(p^2mk+q^2nl-\alpha_{mn}\alpha_{kl})+{}_1M_{k+m,l-n}^{mnkl}(p^2mk-q^2nl+\alpha_{mn}\alpha_{kl})\right.\\ \left.+{}_1M_{k-m,l+n}^{mnkl}(p^2mk-q^2nl-\alpha_{mn}\alpha_{kl})+{}_1M_{k+m,l+n}^{mnkl}(p^2mk+q^2nl+\alpha_{mn}\alpha_{kl})\right]\end{array}\right\}
\end{aligned}
\tag{A3}
$$

${}_1P_{rs}^{mnkl}$ and ${}_1M_{rs}^{mnkl}$ being Fourier coefficients defined by

$$
sh(\alpha_{mn}+\alpha_{kl})(\eta+d_1) = \sum_{u=0}^{\infty}\sum_{v=0}^{\infty}\Delta_{u0}\Delta_{v0}\,{}_1P_{uv}^{mnkl}\cos uX\cos vY
\tag{A4}
$$

$$
sh(\alpha_{mn}+\alpha_{kl})(\eta+d_1) = \sum_{u=0}^{\infty}\sum_{v=0}^{\infty}\Delta_{u0}\Delta_{v0}\,{}_1M_{uv}^{mnkl}\cos uX\cos vY.
\tag{A5}
$$

The second term on the right-hand side of Equation (A1), labelled KE_2, represents the kinetic energy in the upper fluid of the wave. This integral is handled in exactly the same way as for KE_1. The result is

$$
\begin{aligned}
\mathrm{KE}_2 &= -\frac{\mu}{1-\mu}\frac{1}{64}\sum_{m=1}^{\infty}\sum_{n=0}^{\infty}\sum_{k=1}^{\infty}\sum_{l=0}^{\infty}\frac{c_{mn}c_{kl}}{ch(\alpha_{mn}d_2)ch(\alpha_{kl}d_2)} \\
&\times \frac{1}{(\alpha_{mn}+\alpha_{kl})}\left\{\begin{array}{l}\left[{}_2P_{k-m,l-n}^{mnkl}(p^2mk+q^2nl+\alpha_{mn}\alpha_{kl})+{}_2P_{k+m,l-n}^{mnkl}(p^2mk-q^2nl-\alpha_{mn}\alpha_{kl})\right.\\ \left.+{}_2P_{k-m,l+n}^{mnkl}(p^2mk-q^2nl+\alpha_{mn}\alpha_{kl})+{}_2P_{k+m,l+n}^{mnkl}(p^2mk+q^2nl-\alpha_{mn}\alpha_{kl})\right]\end{array}\right\} \\
&- \frac{\mu}{1-\mu}\frac{1}{64}\sum_{m=1}^{\infty}\sum_{n=0}^{\infty}\sum_{k=1}^{\infty}\sum_{l=0}^{\infty}\frac{c_{mn}c_{kl}}{ch(\alpha_{mn}d_2)ch(\alpha_{kl}d_2)} \\
&\times \frac{1}{(\alpha_{mn}-\alpha_{kl})}\left\{\begin{array}{l}\left[{}_2M_{k-m,l-n}^{mnkl}(p^2mk+q^2nl-\alpha_{mn}\alpha_{kl})+{}_2M_{k+m,l-n}^{mnkl}(p^2mk-q^2nl+\alpha_{mn}\alpha_{kl})\right.\\ \left.+{}_2M_{k-m,l+n}^{mnkl}(p^2mk-q^2nl-\alpha_{mn}\alpha_{kl})+{}_2M_{k+m,l+n}^{mnkl}(p^2mk+q^2nl+\alpha_{mn}\alpha_{kl})\right]\end{array}\right\}
\end{aligned}
\tag{A6}
$$

${}_2P_{rs}^{mnkl}$ and ${}_2M_{rs}^{mnkl}$ being Fourier coefficients defined by

$$
sh(\alpha_{mn}+\alpha_{kl})(\eta-d_2) = \sum_{u=0}^{\infty}\sum_{v=0}^{\infty}\Delta_{u0}\Delta_{v0}\,{}_2P_{uv}^{mnkl}\cos uX\cos vY
\tag{A7}
$$

$$
sh(\alpha_{mn}-\alpha_{kl})(\eta-d_2) = \sum_{u=0}^{\infty}\sum_{v=0}^{\infty}\Delta_{u0}\Delta_{v0}\,{}_2M_{uv}^{mnkl}\cos uX\cos vY.
\tag{A8}
$$

Using expressions (A3) and (A6), the kinetic energy can be expressed in a compact form by

$$
\begin{aligned}
\mathrm{KE} &= \frac{1}{64(1-\mu)}\sum_{m=1}^{\infty}\sum_{n=0}^{\infty}\sum_{k=1}^{\infty}\sum_{l=0}^{\infty}\frac{b_{mn}b_{kl}}{ch(\alpha_{mn}d_1)ch(\alpha_{kl}d_1)}\times\frac{1}{(\alpha_{mn}+\alpha_{kl})}[{}_1\Omega_{mnkl}^+]^t[\Theta_{mnkl}^+] \\
&+ \frac{1}{64(1-\mu)}\underbrace{\sum_{m=1}^{\infty}\sum_{n=0}^{\infty}\sum_{k=1}^{\infty}\sum_{l=0}^{\infty}}_{\alpha_{mn}\neq\alpha_{kl}}\frac{b_{mn}b_{kl}}{ch(\alpha_{mn}d_1)ch(\alpha_{kl}d_1)}\times\frac{1}{(\alpha_{mn}-\alpha_{kl})}[{}_1\Omega_{mnkl}^-]^t[\Theta_{mnkl}^-]
\end{aligned}
$$

$$+ \frac{1}{64(1-\mu)} \underbrace{\sum_{m=1}^{\infty} \sum_{n=0}^{\infty} \sum_{k=1}^{\infty} \sum_{l=0}^{\infty}}_{\alpha_{mn}=\alpha_{kl}} \frac{b_{mn}b_{kl}}{ch^2(\alpha_{mn}d_1)} \times [_1\Lambda_{mn}]^t [\Theta^+_{mnmn}]$$

$$- \frac{\mu}{64(1-\mu)} \sum_{m=1}^{\infty} \sum_{n=0}^{\infty} \sum_{k=1}^{\infty} \sum_{l=0}^{\infty} \frac{c_{mn}c_{kl}}{ch(\alpha_{mn}d_2)ch(\alpha_{kl}d_2)} \times \frac{1}{(\alpha_{mn}+\alpha_{kl})} [_2\Omega^+_{mnkl}]^t [\Theta^+_{mnkl}]$$

$$- \frac{\mu}{64(1-\mu)} \underbrace{\sum_{m=1}^{\infty} \sum_{n=0}^{\infty} \sum_{k=1}^{\infty} \sum_{l=0}^{\infty}}_{\alpha_{mn}\neq\alpha_{kl}} \frac{c_{mn}c_{kl}}{ch(\alpha_{mn}d_2)ch(\alpha_{kl}d_2)} \times \frac{1}{(\alpha_{mn}-\alpha_{kl})} [_2\Omega^-_{mnkl}]^t [\Theta^-_{mnkl}]$$

$$- \frac{\mu}{64(1-\mu)} \underbrace{\sum_{m=1}^{\infty} \sum_{n=0}^{\infty} \sum_{k=1}^{\infty} \sum_{l=0}^{\infty}}_{\alpha_{mn}=\alpha_{kl}} \frac{c_{mn}c_{kl}}{ch^2(\alpha_{mn}d_2)} \times [_2\Lambda_{mn}]^t [\Theta^+_{mnmn}] \tag{A9}$$

where we have

$$[\Theta^+_{mnkl}] = \begin{bmatrix} p^2 mk + q^2 nl + \alpha_{mn}\alpha_{kl} \\ p^2 mk - q^2 nl + \alpha_{mn}\alpha_{kl} \\ p^2 mk - q^2 nl - \alpha_{mn}\alpha_{kl} \\ p^2 mk + q^2 nl - \alpha_{mn}\alpha_{kl} \end{bmatrix} \quad [\Theta^-_{mnkl}] = \begin{bmatrix} p^2 mk + q^2 nl - \alpha_{mn}\alpha_{kl} \\ p^2 mk - q^2 nl - \alpha_{mn}\alpha_{kl} \\ p^2 mk - q^2 nl + \alpha_{mn}\alpha_{kl} \\ p^2 mk + q^2 nl + \alpha_{mn}\alpha_{kl} \end{bmatrix}$$

$$[_i\Omega^+_{mnkl}] = \begin{bmatrix} _iP^{mnkl}_{k-m,l-n} \\ _iP^{mnkl}_{k-m,l+n} \\ _iP^{mnkl}_{k+m,l-n} \\ _iP^{mnkl}_{k+m,l+n} \end{bmatrix} \quad (i=1,2) \quad [_i\Omega^-_{mnkl}] = \begin{bmatrix} _iM^{mnkl}_{k-m,l-n} \\ _iM^{mnkl}_{k-m,l+n} \\ _iM^{mnkl}_{k+m,l-n} \\ _iM^{mnkl}_{k+m,l+n} \end{bmatrix} \quad (i=1,2)$$

$$[_i\Lambda_{mn}] = \begin{bmatrix} a_{k-m,l-n} + 4(-1)^i d_i \\ a_{k-m,l+n} \\ a_{k+m,l-n} \\ a_{k+m,l+n} \end{bmatrix}.$$

A.2. *The term of potential energy*

In the right-hand side of (7), the averaged potential energy, V_g, due to gravity only is defined as

$$V_g = \frac{1}{4\pi^2} \int_0^{2\pi} \int_0^{2\pi} \left[\frac{1}{2}\eta^2 \right] \mathrm{d}X\mathrm{d}Y = \frac{1}{8} \sum_{m=0}^{\infty} \sum_{n=0}^{\infty} \Delta_{m0}\Delta_{n0}a_{mn}^2. \tag{A10}$$

On the other hand, for the term of the averaged capillary energy defined by

$$V_\tau = \frac{\kappa}{4\pi^2} \int_0^{2\pi} \int_0^{2\pi} \left(\sqrt{1 + p^2 \left(\frac{\partial \eta}{\partial X} \right)^2 + q^2 \left(\frac{\partial \eta}{\partial Y} \right)^2} - 1 \right) \mathrm{d}X\mathrm{d}Y \tag{A11}$$

we introduce the following Fourier expansion

$$\sqrt{1 + p^2 \left(\frac{\partial \eta}{\partial X} \right)^2 + q^2 \left(\frac{\partial \eta}{\partial Y} \right)^2} = \sum_{m=0}^{\infty} \sum_{n=0}^{\infty} \Delta_{m0}\Delta_{n0}R_{mn} \cos mX \cos nY. \tag{A12}$$

That enables us to compute easily the integral to obtain then

$$V_\tau = \frac{\kappa}{4}(R_{00} - 4). \tag{A13}$$

R_{00} is computed by using the fast Fourier transform (FFT) algorithm.

A.3. *The term of averaged temporal rate of variation of the velocity potentials*

The remaining terms represents the total temporal rate of variation of the potentials and has the following expression

$$\overline{\Phi}_t = -\frac{1}{1-\mu}\frac{1}{4\pi^2}\int_0^{2\pi}\int_0^{2\pi}\int_{-d_1}^{\eta}\varpi\,\Phi_{1X}\mathrm{d}Z\mathrm{d}X\mathrm{d}Y - \frac{\mu}{1-\mu}\frac{1}{4\pi^2}\int_0^{2\pi}\int_0^{2\pi}\int_{\eta}^{d_2}\varpi\,\Phi_{1X}\mathrm{d}Z\mathrm{d}X\mathrm{d}Y. \quad \text{(A14)}$$

After substituting the expansions (12) and (13) into (A14), and after integration with respect to Z, one obtains

$$\overline{\Phi}_t = -\frac{1}{1-\mu}\frac{\varpi}{4\pi^2}\sum_{m=1}^{\infty}\sum_{n=0}^{\infty}m\frac{b_{mn}}{\alpha_{mn}}\int_0^{2\pi}\int_0^{2\pi}\frac{sh(\alpha_{mn}(\eta+d_1))}{ch(\alpha_{mn}d_1)}\cos mX\cos nY\mathrm{d}X\mathrm{d}Y$$

$$+\frac{\mu}{1-\mu}\frac{\varpi}{4\pi^2}\sum_{m=1}^{\infty}\sum_{n=0}^{\infty}m\frac{c_{mn}}{\alpha_{mn}}\int_0^{2\pi}\int_0^{2\pi}\frac{sh(\alpha_{mn}(\eta-d_2))}{ch(\alpha_{mn}d_2)}\cos mX\cos nY\mathrm{d}X\mathrm{d}Y. \quad \text{(A15)}$$

The integrals of the right-hand-side suggest to use the coefficients of Fourier's expansion of $sh(\alpha_{mn}(\eta+d_1))$ and $sh(\alpha_{mn}(\eta-d_2))$, that is;

$$sh(\alpha_{mn}(\eta+d_1)) = \sum_{i=0}^{\infty}\sum_{j=0}^{\infty}\Delta_{i0}\Delta_{j0}(_1\omega_{ij}^{mn})\cos iX\cos jY$$

$$sh(\alpha_{mn}(\eta-d_2)) = \sum_{i=0}^{\infty}\sum_{j=0}^{\infty}\Delta_{i0}\Delta_{j0}(_2\omega_{ij}^{mn})\cos iX\cos jY.$$

In doing so, $\overline{\Phi}_t$ is easily found as

$$\overline{\Phi}_t = -\frac{1}{1-\mu}\frac{\varpi}{4}\sum_{m=1}^{\infty}\sum_{n=0}^{\infty}m\frac{b_{mn}}{\alpha_{mn}ch(\alpha_{mn}d_1)}{}_1\omega_{mn}^{mn} + \frac{\mu}{1-\mu}\frac{\varpi}{4}\sum_{m=1}^{\infty}\sum_{n=0}^{\infty}m\frac{c_{mn}}{\alpha_{mn}ch(\alpha_{mn}d_2)}{}_2\omega_{mn}^{mn}. \quad \text{(A16)}$$

Using expressions (A9), (A10), (A13), and (A16), the averaged Lagrangian function is obtained as a function of the coefficients and can be written in the form

$$\overline{L} = \frac{1}{64(1-\mu)}\sum_{m=1}^{\infty}\sum_{n=0}^{\infty}\sum_{k=1}^{\infty}\sum_{l=0}^{\infty}\frac{b_{mn}b_{kl}}{ch(\alpha_{mn}d_1)ch(\alpha_{kl}d_1)}\times\frac{1}{(\alpha_{mn}+\alpha_{kl})}[_1\Omega_{mnkl}^+]^t[\Theta_{mnkl}^+]$$

$$+\frac{1}{64(1-\mu)}\underbrace{\sum_{m=1}^{\infty}\sum_{n=0}^{\infty}\sum_{k=1}^{\infty}\sum_{l=0}^{\infty}}_{\alpha_{mn}\neq\alpha_{kl}}\frac{b_{mn}b_{kl}}{ch(\alpha_{mn}d_1)ch(\alpha_{kl}d_1)}\times\frac{1}{(\alpha_{mn}-\alpha_{kl})}[_1\Omega_{mnkl}^-]^t[\Theta_{mnkl}^-]$$

$$+\frac{1}{64(1-\mu)}\underbrace{\sum_{m=1}^{\infty}\sum_{n=0}^{\infty}\sum_{k=1}^{\infty}\sum_{l=0}^{\infty}}_{\alpha_{mn}=\alpha_{kl}}\frac{b_{mn}b_{kl}}{ch^2(\alpha_{mn}d_1)}\times[_1\Lambda_{mn}]^t[\Theta_{mnmn}^+]$$

$$-\frac{\mu}{64(1-\mu)}\sum_{m=1}^{\infty}\sum_{n=0}^{\infty}\sum_{k=1}^{\infty}\sum_{l=0}^{\infty}\frac{c_{mn}c_{kl}}{ch(\alpha_{mn}d_2)ch(\alpha_{kl}d_2)}\times\frac{1}{(\alpha_{mn}+\alpha_{kl})}[_2\Omega_{mnkl}^+]^t[\Theta_{mnkl}^+]$$

$$-\frac{\mu}{64(1-\mu)}\underbrace{\sum_{m=1}^{\infty}\sum_{n=0}^{\infty}\sum_{k=1}^{\infty}\sum_{l=0}^{\infty}}_{\alpha_{mn}\neq\alpha_{kl}}\frac{c_{mn}c_{kl}}{ch(\alpha_{mn}d_2)ch(\alpha_{kl}d_2)}\times\frac{1}{(\alpha_{mn}-\alpha_{kl})}[_2\Omega_{mnkl}^-]^t[\Theta_{mnkl}^-]$$

$$-\frac{\mu}{64(1-\mu)}\underbrace{\sum_{m=1}^{\infty}\sum_{n=0}^{\infty}\sum_{k=1}^{\infty}\sum_{l=0}^{\infty}}_{\alpha_{mn}=\alpha_{kl}}\frac{c_{mn}c_{kl}}{ch^2(\alpha_{mn}d_2)}\times[_2\Lambda_{mn}]^t[\Theta_{mnmn}^+]$$

$$+\frac{1}{8}\sum_{m=0}^{\infty}\sum_{n=0}^{\infty}\Delta_{m0}\Delta_{n0}a_{mn}^2 - \frac{1}{4(1-\mu)}\varpi\sum_{m=1}^{\infty}\sum_{n=0}^{\infty}m\frac{b_{mn}}{\alpha_{mn}ch(\alpha_{mn}d_1)}{}_1\omega_{mn}^{mn}$$

$$+\frac{\mu}{4(1-\mu)}\varpi\sum_{m=1}^{\infty}\sum_{n=0}^{\infty}m\frac{c_{mn}}{\alpha_{mn}ch(\alpha_{mn}d_2)}{}_2\omega_{mn}^{mn} + \frac{\kappa}{4}(R_{00}-4). \quad \text{(A17)}$$

The details of first and second derivatives of the averaged lagrangian are available from the authors. They are useful to calculate the terms of the variational equations (18) and (19) and to solve them.

References

[1] R. A. Fuchs, "On the theory of short–crested oscillatory waves. Gravity waves", *U.S. Natl. Bur. Stand. Circ.* **521** (1952), p. 187-200.

[2] J. R. C. Hsu, Y. Tsuchiya, R. Silvester, "Third order approximation to short-crested waves", *J. Fluid Mech.* **90** (1979), p. 179-196.

[3] A. J. Roberts, "Highly nonlinear short-crested water waves", *J. Fluid Mech.* **135** (1983), p. 323-335.

[4] M. Ioualalen, "Fourth order approximation of short-crested waves", *C. R. Acad. Sci. Paris, Sér. II* **316** (1993), p. 1193-1200.

[5] O. KImmoun, H. Branger, C. Kharif, "On short-crested waves: experimental and analytical investigations", *Eur. J. Mech. B/Fluids* **18** (1999), p. 889-930.

[6] W. Craig, D. P. Nicholls, "Travelling two and three dimensional capillary gravity water waves", *SIAM J. Math. Anal.* **32** (2000), p. 323-359.

[7] W. Craig, D. P. Nicholls, "Traveling gravity water waves in two and three dimensions", *Eur. J. Mech. B/Fluids* **21** (2002), p. 615-641.

[8] A. J. Roberts, L. W. Schwartz, "The calculation of nonlinear short-crested gravity waves", *Phys. Fluids* **26** (1983), p. 2388-2392.

[9] M. Okamura, "Notes on short-crested waves in deep water", *J. Phys. Soc. Jpn.* **65** (1996), p. 2841-2845.

[10] M. Okamura, "Almost limiting short-crested gravity waves in deep water", *J. Fluid Mech.* **646** (2010), p. 481-503.

[11] M. Debiane, C. Kharif, "Calculation of resonant short-crested waves in deep water", *Eur. J. Mech. B/Fluids* **21** (2009), p. 1-12.

[12] N. Allalou, M. Debiane, C. Kharif, "Three-dimensional periodic interfacial gravity waves: Analytical and numerical results", *Eur. J. Mech. B/Fluids* **30** (2011), p. 371-386.

[13] A. A. Bocharov, G. A. Khabakhpashev, O. Yu. Tsvelodub, "Numerical simulation of plane and spatial nonlinear stationary waves in a two-layer fluid of arbitrary depth", *Fluid Dyn.* **43** (2008), p. 118-124.

[14] G. A. Khabakhpashev, O. Yu. Tsvelodub, "Evolutionary equation for weakly nonlinear waves in a two-layer fluid with slightly sloping bottom and cover", *Prikl. Mekh. Tekhn. Fiz.* **40** (1999), p. 62-72.

[15] G. B. Whitham, *Linear and Nonlinear Waves*, Wiley-Interscience, New York, 1974.

[16] J. R. Wilton, "On ripples", *Philos. Mag.* **29** (1915), p. 688-700.

[17] H. Segur, "Integrable models of waves in shallow water", *Probab. Geom. Integr. Syst.* **55** (2007), p. 345-371.

[18] J. L. Hammack, D. M. Henderson, H. Segur, "Progressive waves with persistent two-dimensional surface patterns in deep water", *J. Fluid Mech.* **532** (2005), p. 1-52.